A Sigmoid-Based Optimization Approach for Multi-UAV-Aided IRS-Assisted Quantum Entanglement Distribution in FSO Networks

Giovanni Iacovelli, *Member, IEEE*, Francesco Vista, *Member, IEEE*, Stephen DiAdamo, and Symeon Chatzinotas, *Fellow, IEEE*

***Abstract*—Quantum networks connect devices to facilitate the transmission of quantum bits (qubits), harnessing quantum mechanics for groundbreaking telecommunications applications. The quantum state exchange rely on quantum entangled particles which have to be sent from a Quantum Base Station (QBS) to Quantum Nodes (QNs) through an optical channel. Free Space Optical (FSO) links promise flexibility and cost advantages over the classical fiber-based infrastructure. However, the absence of Line of Sight (LoS) between the QBS and QNs may completely disrupt the communication. Therefore, this work focuses on an Intelligent Reflective Surface (IRS)-assisted Unmanned Aerial Vehicle (UAV)-aided FSO quantum network. An optimization problem is formulated to fairly maximize qubit reception at QNs by optimizing UAV hovering locations, constrained by fidelity and link-per-IRS limits. The intractability of the original problem is first tackled with a sigmoid-based approximations, subsequently split into three sub-problems, sequentially solved applying the Successive Convex Approximation (SCA) technique. Numerical results (i) validate the approximation accuracy, and (ii) demonstrates the effectiveness of the proposal against three baseline approaches, showing an order of magnitude increase in terms of fairness.**

***Index Terms*—Internet of Drones, Intelligent Reflective Surface, Quantum Entanglement, Optimization.**

I. Introduction

QUANTUM networks, i.e., a system of interconnected quantum devices, promise to extend the capabilities of classical networks [1]–[3] by enabling the transmission of quantum states, i.e., quantum bits (qubits). The unique characteristics inherited from quantum mechanics allow for the realization of emerging and relevant applications, such as distributed quantum computing [4]–[7], secure communication via Quantum Key Distribution (QKD) [8]–[10] and quantum teleportation [11]–[13], quantum clock synchronization [14], [15], and distributed quantum sensing [16]. All quantum communication protocols, at the basis of the aforementioned applications, hinge on the unique properties of sharing quantum entanglement between Quantum Nodes (QNs). Quantum entanglement is a phenomenon exhibited by systems of quantum particles, where the state of one particle instantly affects the state of another, regardless of the distance in between [17].

Although quantum entanglement is a crucial resource in quantum networks, distributing it over long distances remains a significant and challenging milestone toward the deployment of large-scale quantum networks [18]. One of the main obstacles is to guarantee a high entanglement fidelity, a measure of how accurately a quantum state is preserved, which can be subject to degradation introduced by the interaction with the environment [19]. Additionally, the intrinsic properties of quantum mechanics do not allow the quantum signal to be amplified or copied, requiring strategies very different from those used in classical networks [20].

Typically, entanglement is generated by using different methodologies, such as the Spontaneous Parametric Down-Conversion (SPDC) process, which generates a pair of polarization-entangled photons [18]. Then, they are distributed through a quantum channel, via optical fibers or Free Space Optical (FSO) links.

Fiber-based channels have the advantage that environmental factors have minimal impact, thus preserving the coherence of photons [21]. However, the success probability of transmitting these optical signals decreases exponentially with increasing distance [13]. To overcome this, an analogue of the classical repeater, known as a quantum repeater, must be employed [22]. Quantum repeaters break the long quantum channel into segments, creating entanglement between adjacent nodes and merging non-adjacent links through a process called entanglement swapping [23]. In this case, the drawback is that the swapping operation is probabilistic and the fidelity of the entangled states generally decreases with the number of swaps involved [24]. Additionally, fiber-based quantum networks are constrained by the availability of fiber connections, which can be challenging to set up in areas with natural barriers.

In FSO-based quantum networks, quantum optical signals are transmitted wirelessly through free space, offering greater flexibility and cost efficiency, in terms of infrastructure, compared to optical fiber networks. However, different environmental factors, such as beam diffraction, pointing error, atmospheric turbulence, absorption, and beam divergence, may increase signal loss and affect its quality [25], [26].

Over the last decade, different experiments showcased the feasibility of distributing entanglement through satellite-to-ground [27], [28] FSO channel. Notably, the Micius satel-

G. Iacovelli, F. Vista, and S. Chatzinotas are with the Signal Processing and Communications (SIGCOM) Research Group at Interdisciplinary Centre for Security, Reliability and Trust (SnT), University of Luxembourg, 1855 Luxembourg City, Luxembourg (email: giovanni.iacovelli@uni.lu, francesco.vista@uni.lu, and symeon.chatzinotas@uni.lu). S. DiAdamo is with Qoro Quantum, Munich, Germany, 81737 (email: stephen.diadamo@gmail.com). This work is funded by the Luxembourg National Research Fund (FNR) under project RISOTTI C20/IS/14773976.

lite [29] has enabled entangled photon distribution between two ground stations over a distance greater than 1000 km. However, satellites can establish quantum channels for certain ground locations only for limited time windows [30], [31], necessitating an ad-hoc constellation to ensure continuous entanglement distribution [32].

A terrestrial Quantum Base Station (QBS) [33] is a cost-efficient near-term solution to provide continuous entanglement service via FSO channel to QNs that are not reachable by fiber. However, a fundamental challenge arises when the direct pathway between the QBS and QNs is obstructed by an obstacle. Without Line of Sight (LoS), the highly focused and directional nature of optical signals makes it impossible to transmit over an FSO channel between distant nodes. To address this issue, Intelligent Reflective Surface (IRS), also known as Reconfigurable Intelligent Surface (RIS), can be adopted [34]. These metasurfaces are composed of passive elements capable of autonomously adjusting critical parameters of incident signals, such as amplitude, frequency, phase, and polarization [35]. Typically deployed on ceilings or walls, IRS can reflect signals to establish a virtual LoS, effectively mitigating dead zones. An alternative solution can be the usage of a swarm of Unmanned Aerial Vehicles (UAVs) to easily establish wireless connections. They can be positioned to form a relay network, ensuring that entangled photons can bypass obstacles and reach their intended QNs [30], [36].

A. Related Works

IRS have received considerable attention for enhancing the performance of future wireless communication systems operating at microwave, mmWave, and terahertz frequencies [37]. Some recent works have also considered the applicability of optical IRS to alleviate the LoS requirement in FSO-based quantum networks. Specifically, authors in [38] investigated an IRS-assisted single point-to-point Non Line of Sight (NLoS) FSO quantum communication system for distributing secret keys. Conversely, in [39], authors examined a multi-user network secured by QKD. However, both works, did not consider the impact of environmental effects on the losses and fidelity of quantum states, and they also assume that the generation of QKD keys is always successful. A representative study addressing these gaps was proposed in [40], which derived a closed-form expression for the probability of successfully transmitting entangled photons and their fidelity while travelling a FSO terrestrial channel with various environmental effects. They also optimize the position of the IRS to assist the entanglement distribution from a central quantum source to a multi-user quantum network. Despite the very interesting mathematical results obtained in this work, the formulated optimization problem is solved with a heuristic algorithm, thus not tackling the non-convexity properly. Moreover, it overlooks a deep analysis of the achievable performance in the case of multiple IRSs.

Another promising solution consists of the employment of a swarm of UAVs to mitigate NLoS issues between communicating nodes. Previous works have utilized drones to share secret keys generated through different QKD protocols to distant nodes [41], [42]. Recently, instead, drone-based quantum links have already been demonstrated for entanglement distribution, showing a robust transmission of single photons [30], [36]. In these works, the entanglement is generated onboard the drone and transmitted via FSO channel to the ground users. To extend the communication path, multiple UAVs should act as quantum repeaters and perform entanglement swapping operations, which, in order to be performed in a precisely timed manner, require additional computation overhead and control schemes, such as Software-Defined Networking (SDN) technology [43].

B. Motivations

FSO links offer a promising solution for entanglement distribution in quantum networks, eliminating the need for the extensive physical infrastructure required by fiber-based systems. In addition, FSO provides strong security, as intercepting an optical beam without detection is extremely challenging.

However, a key limitation of FSO systems is their strict LoS requirement. To address this challenge, integrating IRS technology with UAVs offers a dynamic and adaptable solution. UAVs can be deployed to improve LoS conditions, reduce path loss, and enhance channel quality, while IRSs enable the intelligent redirection of optical signals, ensuring robust entanglement distribution even in complex environments.

The use of a swarm of IRS-equipped UAVs further enhances network flexibility, allowing for real-time adaptation to changing topologies. UAVs can be repositioned to optimize link quality and coverage, while depleted units can be seamlessly replaced to maintain continuous operation.

To the best of the authors' knowledge, no existing work considers the integration of a swarm of IRS-equipped UAVs in FSO-based quantum networks for entanglement distribution.

C. Contributions

Starting from the discussion above, the main contributions of this paper are outlined below.

- The mathematical system model associated with a IRS-assisted UAV-aided FSO quantum network is derived, also accounting for the QBS-IRS-QN channel model. Specifically, the probability of successfully receiving a qubit and its fidelity are expressed as functions of attenuation- and noise-related phenomena.
- Starting from the above, an optimization problem is formulated to fairly maximize the number of qubits received by all QNs and jointly optimize (i) the locations of the UAVs, and (ii) the scheduling plan, describing how many entangled pairs should be allocated at each node couple, subject to a minimum fidelity and a maximum link-per-IRS constraints. Unlike existing studies, which often relax the integer constraints, our approach explicitly addresses them using Heaviside and ℓ_0-norm functions, enabling a continuous-domain optimization variables.
- The original non-convex formulation is tackled through a dedicated optimization strategy. First, the integer non-continuous terms are approximated through the sigmoid function. Then, the original problem is split into

three sub-problems are sequentially solved employing the Successive Convex Approximation (SCA) technique until convergence to prescribed accuracy.
- The time complexity of the whole optimization algorithm is analyzed, accounting for the number of drones and QNs in different topologies. Additionally, the unavoidable sub-optimality of the proposed algorithm, which stems from the intrinsic complexity of the problem, and the adopted approximations are discussed.
- Numerical simulations are provided to assess (i) the accuracy of the approximations, and (ii) the effectiveness of the proposed optimization strategy. In particular, the latter is extensively analyzed under different scenario conditions. Moreover, the proposed algorithm is evaluated against three baseline strategies: two that adopt weighted k-means clustering for UAV placement combined with heuristic resource allocation methods, and a third that performs a brute-force grid search under a closed-form allocation model.

The simulation campaign clearly indicates that the number of UAVs employed and the number of link-per-IRS can provide a substantial increment in performance for a fixed mission time duration. The effectiveness of the proposal in terms of fairness is demonstrated by an improvement of an order of magnitude compared to the first two baselines, while consistently achieving minimum rates comparable to the third.

D. Paper outline and notations

The paper is organized as follows. Section II introduces the system model, describing optical channel and quantum noises. Starting from the model, Section III outlines the problem formulation. Section IV presents the sigmoid-based approximation. Section V proposes an optimization algorithm to address the problem. The complexity of the algorithm and its optimality are analyzed in Section VI. Section VII presents the results under different configuration scenarios and compares them against three baseline approaches. Finally, Section VIII concludes the work and draws future research perspectives.

Boldface lower case letters refer to vectors; $\mathbf{x}^{\mathsf{T}}$ is the transpose of a generic vector $\mathbf{x}$; $|\mathbf{x}\rangle$ is the column vector of a generic quantum state $\mathbf{x}$; $\mathcal{O}(x)$ denotes the time-complexity of an algorithm of input size x, i.e, big-O notation. The main adopted symbols of this paper are summarized in Table I.

II. System Model

This work envisions a FSO quantum network, depicted in Figure 1, composed of a QBS, located at $\mathbf{b} \in \mathbb{R}^3$, and a group of K QNs, each one placed in a known position $\mathbf{u}_k \in \mathbb{R}^3$ with $k = 1, \dots, K$. It is assumed that the direct LoS FSO quantum links between the QBS and quantum nodes are obstructed due to the presence of blockage, e.g., buildings. To establish a virtual LoS link between the QBS and quantum nodes, a swarm of N IRS-equipped UAVs is considered [44]. The NLoS channel component is therefore neglected since (i) Air-to-Ground communications are predominantly governed by LoS condition and (ii) such contributions experience severe path loss due to the high carrier frequency. The entire mission is uniformly split into T timeslots of duration δ seconds each. The UAVs hover over a fixed position, denoted by $\mathbf{q}_n = [x_n, y_n]^{\mathsf{T}} \in \mathbb{R}^2$, at a fixed altitude $z_n = z$. Furthermore, the QBS is equipped with the necessary entanglement generation devices to serve each QBS-IRS-QN link [45] at a rate $r_{t,n,k} \geq 0$ photon pairs per second, with $\sum_{n,k} r_{t,n,k} \leq R_{MAX}$, $\forall t = 1, \dots, T$. Half of each pair is stored within the QBS quantum memory, while the other half is transmitted over the FSO channel to the quantum nodes. Hence, the end-to-end (E2E) distance between the QBS and a quantum node k through a UAV n is $d_{n,k} = \left\|[\mathbf{q}_n, z]^{\mathsf{T}} - \mathbf{u}_k\right\| + \left\|[\mathbf{q}_n, z]^{\mathsf{T}} - \mathbf{b}\right\|$, which is clearly the sum of the distance of the two paths. Since the QNs positions are known, the phase-shift matrix of each IRS is tuned such that the entangled photons are reflected in the desired direction. Moreover, since the considered distances are far greater than the actors involved, the far-field assumption is adopted [40].

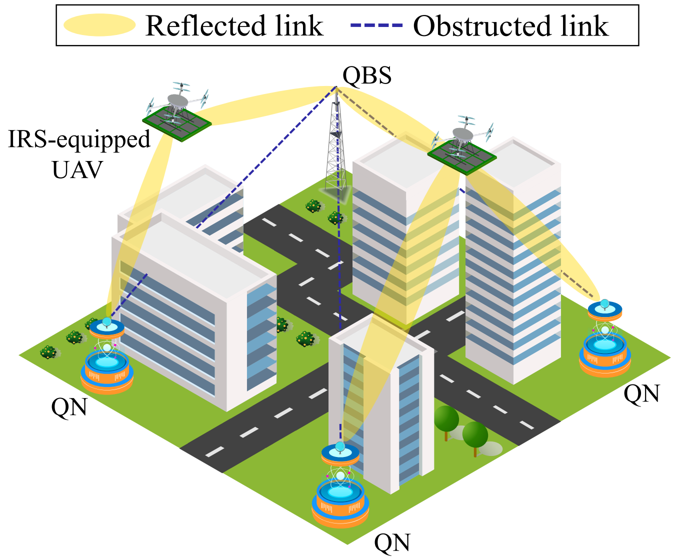

Fig. 1: FSO-based IRS-assisted multi-UAV quantum network.

A. Optical channel

The states transmitted over the FSO channel may be lost due to several environmental effects which are all strictly dependent on the position of the UAVs, i.e., the distance traveled by photons. According to [40], the probability of successfully sending an entangled photon over the QBS-IRS-QN FSO quantum channel considering the atmospheric loss [46], moderate turbulence [47], and pointing error [26] is

$$p_{n,k} = 1 - \left(\gamma_{n,k} G_{2,4}^{3,1}\left[\frac{\alpha_{n,k}\beta_{n,k}\chi}{A_{n,k}h_{n,k}} \,\middle|\, \begin{smallmatrix} 1,\vartheta_{n,k}+1 \\ \vartheta_{n,k},\alpha_{n,k},\beta_{n,k},0 \end{smallmatrix}\right]\right) \quad (1)$$

with

$$\alpha_{n,k} = \exp^{-1}\left(0.49\sigma_{n,k}^2/(1+1.11\sigma_{n,k}^{\frac{12}{5}})^{7/6}\right), \quad (2)$$

$$\beta_{n,k} = \exp^{-1}\left(0.51\sigma_{n,k}^2/(1+0.69\sigma_{n,k}^{\frac{12}{5}})^{5/6}\right), \quad (3)$$

$$\gamma_{n,k} = \vartheta_{n,k}/(\Gamma(\alpha_{n,k})\Gamma(\beta_{n,k}))^{-1} \quad (4)$$

Symbol	Description	Symbol	Description
K	Number of QN deployed on the ground.	$\vartheta_{n,k}$	Pointing errors due to the beam jitter at the transmitter.
N	Number of IRS-equipped UAVs.	$A_{n,k}$	Pointing errors due to the beam jitter at the IRS.
T	Number of discrete timeslots of the mission.	$h_{n,k}$	The atmospheric attenuation.
δ	Timeslot duration.	$p_{n,k}$	Probability of successfully sending an entangled photon.
$\mathbf{u}_k$	Location of the k-th QN.	$a_{n,k}$	Binary variable representing the UAV-QN association.
$\mathbf{b}$	Location of the QBS.	ζ_{th}	FSO channel threshold.
$\mathbf{q}_n$	Horizontal location of the n-th IRS-equipped UAV.	ς	IRS reflection efficiency.
z	Altitude of the n-th IRS-equipped UAV.	ν	Responsivity of the receiver.
ℓ	The wavelength.	$\rho_{n,k}$	Density matrix of the initial Bell-diagonal state.
$d_{n,k}$	Distance between the QBS and the k-th QN.	$\|\Phi^+\rangle$	Reference Bell state.
$r_{t,n,k}$	Entangled photons generation rate by the QBS.	$\boldsymbol{\sigma}_X$, $\boldsymbol{\sigma}_Z$	Pauli X and Pauli Z gates.
R_{MAX}	Maximum entanglement generation rate of the QBS.	$\tilde{t}_{n,k}$	Storage time of entangled photons.
$\alpha_{n,k}$	The inverse of the variance of the small-scale fading terms.	τ_{coh}	Quantum memory coherence time.
$\beta_{n,k}$	The inverse of the variance of the large-scale fading terms.	τ	Qubit processing time.
$\sigma^2_{n,k}$	The Rytov variance.	c	The speed of light.
κ	The wave number.	$\hat{\rho}_{n,k}$	Resulting density matrix of the received entangled state.
C^2	The refractive index structure constant.	$f_{n,k}$	Resulting fidelity of the received entangled state.
K_{MAX}	Maximum number of nodes served by the same UAV.	f_{min}	The minimum fidelity threshold.

TABLE I: Main notation adopted in this work.

where $\alpha_{n,k}$ and $\beta_{n,k}$ represent, respectively, the inverse of the variance of the small-scale and large-scale turbulent fading terms, $\Gamma(\cdot)$ is the Gamma function, $G^{p,q}_{m,n}[\cdot|\cdot]$ denotes the Meijer G-function, and $\chi = \frac{\zeta_{th}}{\varsigma\nu}$. The Rytov variance $\sigma^2_{n,k} = 1.23C^2\kappa^{7/6}d^{11/6}_{n,k}$ models the phase noise cause by the turbulence, with $\kappa = 2\pi/\ell$ being the wave number, ℓ the corresponding wavelength, and C^2 the refractive index structure constant. This implies that as the distance $d_{n,k}$ increases, turbulence-induced phase noise becomes more significant, reducing the success probability. Moreover, $\vartheta_{n,k}$ and $A_{n,k}$ account for the pointing errors due to the beam jitter at the transmitter and at the IRS, which are caused by mechanical vibrations. $h_{n,k}$, instead, represents the atmospheric attenuation caused by the scattering and absorption of light by particles in the atmosphere [35]. Both pointing errors and atmospheric attenuation degrade the success probability over longer distances. These factors collectively establish a clear dependence of $p_{n,k}$ on distance.

For more details the reader is referred to [26], [40], [48]. It is worth noting that (1), provided the proper IRS phase-shift configuration tuned to point towards the desired QNs, does not depend on the physical characteristics of the IRSs, e.g., size and number of elements. This is due to the far-field regime which implies the so-call point source assumption [40].

Hence, the E2E rate of successfully received qubits for quantum node k is given by $p_{n,k}r_{t,n,k}$.

B. Quantum noise

Given a certain timeslot t and UAV n, the QBS generates pairs of entangled qubits in order to communicate with a quantum node k. The state of entangled photons can be described using a Bell-diagonal state [49], which is represented by the density matrix:

$$\rho_{n,k} = \varphi_{00,nk}\mathbf{\Phi}_{00}+\varphi_{01,nk}\mathbf{\Phi}_{01}+\varphi_{10,nk}\mathbf{\Phi}_{10}+\varphi_{11,nk}\mathbf{\Phi}_{11}, \quad (5)$$

where $\mathbf{\Phi}_{j,l} = |\Phi_{j,l}\rangle\langle\Phi_{j,l}|$ are projectors onto the Bell states $|\Phi_{j,l}\rangle$. The Bell states can be obtained by applying Pauli gates to the reference Bell state $|\Phi^+\rangle$ as $|\Phi_{j,l}\rangle = (\boldsymbol{\sigma}^j_X\boldsymbol{\sigma}^l_Z\otimes\mathbf{I})\,|\Phi^+\rangle$, where $\boldsymbol{\sigma}_X$ and $\boldsymbol{\sigma}_Z$ are the Pauli X- and Z-gates, $\mathbf{I}$ is the identity operator, and $|\Phi^+\rangle = \frac{1}{\sqrt{2}}(|00\rangle + |11\rangle)$. Here, $j, l \in 0, 1$ indicates whether the the Pauli X- and Z-gates are applied, respectively. Moreover, $\varphi_{jl,nk}$ are the fidelity values of the Bell-diagonal state with respect to $\Phi_{j,l}$, provided that $\sum_{j,l\in\{0,1\}}\varphi_{jl,nk} = 1,\ \forall n, k$.

To be able to carry the quantum state and to ensure the reliability of quantum information processing, the entanglement must satisfy a high fidelity which however is mined by the noise experienced by each qubit [49]. Therefore, to properly model the E2E overall fidelity, it is necessary to take into account the storage time that affects the qubits at the QBS and the transmission over the FSO channel that affects the flying qubit.

On one hand, the noise experienced by the stored qubit of the entangled pair, modeled as a depolarizing quantum noise channel [40], depends on the hardware characteristics of the quantum memory, i.e., the memory coherence time τ_{coh}, and the storage time $\tilde{t}_{n,k}$.

The latter is the sum of the travel time of the flying qubit over the FSO channel and the processing time τ of the successfully received qubit at quantum node k, i.e., $\tilde{t}_{n,k} = \frac{d_{n,k}}{c} + \tau$, where c is the speed of light. It is worth mentioning that $\tilde{t}_{n,k} \ll \delta$, thus in the same timeslot multiple qubits are sent.

On the other hand, the major impairment for the flying qubit is the atmospheric turbulence which results in significant phase shift and it is modeled as phase damping quantum noise channel [40]. Specifically, the resulting E2E density matrix of the successfully distributed entangled state $\hat{\rho}_{n,k}$ to the a quantum node can be modeled as [40]:

$$\hat{\rho} = \sum_{j,l\in\{0,1\}} f_{jl,i}\mathbf{\Phi}_{jl}, \quad (6)$$

$$f_{jl,i} = (1-\mathrm{erf}(\sigma^2_{n,k}))g_{jl} + \mathrm{erf}(\sigma^2_{n,k})g_{j(1-l)}, \quad (7)$$

where $\mathrm{erf}(\sigma^2_{n,k})$ represents the damping probability, $g_{j,l} = \left(\frac{1}{4} + (\varphi_{jl,i} - \frac{1}{4})e^{-\tilde{t}_{n,k}/\tau_{coh}}\right)$, and $g_{00}+g_{01}+g_{10}+g_{11} = 1$. Here, the term $e^{-\tilde{t}_{n,k}/\tau_{coh}}$ describes the natural decay of coherence over time, meaning that a longer travel and storage time increase the probability that the qubit will decohere and be replaced by a mixed state.

Without loss of generality, in the sequel of this article, $f_{00,i} \triangleq f_{n,k}$ is chosen as the reference fidelity associated with the state intended to be sent, i.e, $j = l = 0$.

III. Problem Formulation

The objective of this work is to fairly maximize the photons delivered to the nodes, while jointly optimizing the positions of the UAVs. To achieve such an objective, define $\mathbf{Q} = \{\mathbf{q}_n\}$, $\mathbf{R} = \{\mathbf{r}_{t,n} \geq 0\}$, $\mathbf{r}_{t,n} = [r_{t,n,1}, \ldots, r_{t,n,K}]^\mathsf{T}$, and $\mathcal{H}(\cdot)$ as the Heaviside function. Hence, the optimization problem reads:

$$\max_{\eta,\mathbf{Q},\mathbf{R}} \eta \quad s.t. \tag{8}$$

$$\eta \leq \sum_{t=1}^{T} \sum_{n=1}^{N} p_{n,k} r_{t,n,k}, \quad \forall k = 1, \ldots, K, \tag{8a}$$

$$\mathcal{H}(r_{t,n,k}) f_{min} \leq f_{n,k}, \quad \begin{array}{c} \forall t = 1, \ldots, T, \forall n = 1, \ldots, N, \\ \forall k = 1, \ldots, K, \end{array} \tag{8b}$$

$$\sum_{n=1}^{N} \sum_{k=1}^{K} r_{t,n,k} \leq R_{MAX}, \quad \forall t = 1, \ldots, T, \tag{8c}$$

$$\|\mathbf{r}_{t,n}\|_0 \leq K_{MAX}, \quad \forall t = 1, \ldots, T, \forall n = 1, \ldots, N, \tag{8d}$$

where η is an auxiliary variable which allows a fair allocation of the received photons distributed among the nodes, at the end of the mission, realized through constraint (8a). The latter is strictly dependent on the data rate generated by the QBS $r_{t,n,k}$ and the position of the n-th drone via $p_{n,k}$. Further, (8b) guarantees that, whenever the data rate for a quantum node k is non-zero, a minimum fidelity f_{min} is provided. Constraints (8c) and (8d) impose an upper-bound on the maximum generation rate of the QBS R_{MAX} and the maximum number of nodes K_{MAX} which can be simultaneously served (through different regions of the IRS) by the same UAV.

Although all variables involved are continuous, the use of discontinuous functions such as the Heaviside step function $\mathcal{H}(\cdot)$ and the ℓ_0-norm effectively induces binary behavior, enforcing sparsity and selection constraints that recall integer decision variables. Specifically, it presents highly non-linear and non-convex constraints, which makes its present form intractable. In particular, (8a) couples the probability of successfully receiving a photon in (1), and hence a UAV position $\mathbf{q}_n$, with the corresponding data rate of the served quantum node. Moreover, the latter probability expression is difficult to manipulate due to the presence of the Meijer G-function. The UAV position and the data rate are coupled in constraint (8a). Furthermore, constraint (8b) bonds the Heaviside function of the rate with the fidelity $f_{n,k}$, while (8d) involves the zero-norm of a vector.

The inherent combinatorial structure of Problem (8) makes it NP-hard, which can be seen from two simple perspectives. If the UAV positions $\{\mathbf{q}_n\}$ are fixed, the remaining allocation of rates $\{r_{t,n,k}\}$ under capacity and sparsity constraints closely resembles the Generalized Assignment Problem (GAP). Conversely, if the rates are fixed (or treated as binary service indicators), optimizing UAV placements under coverage and capacity constraints yields a continuous analogue of the Capacitated Facility Location Problem (CFLP). Since both GAP and CFLP are classical NP-hard problems, it follows that Problem (8) inherits the same intractability. This intuition is formalized by proving NP-hardness via a polynomial-time reduction from the CFLP decision problem.

Lemma 1. *Problem* (8) *is NP-hard.*

Proof. We prove NP-hardness by reduction from the capacitated covering / facility location decision problem, which is known to be NP-hard. Consider the restriction of Problem (8) in which: (i) the set of feasible UAV positions is limited to a finite set of candidate locations (one per facility), (ii) per-UAV capacity parameters are set equal to the facility capacities, and (iii) per-link rates are constrained to be either 0 or 1 (by setting $R_{min} = R_{MAX} = 1$). Furthermore, the physical parameters are chosen so that a UAV can provide entanglement to a QN if and only if the distance between them is below a prescribed threshold (implemented by fixing the physical/fidelity parameters). Under this construction, deciding whether all QNs can be served is exactly equivalent to the capacitated facility location / capacitated covering problem, which is a classical NP-hard problem. Because this NP-hard problem appears as a special case of (8), it follows that Problem (8) is NP-hard in general. ∎

Clearly, all these issues which make the problem non-convex require a dedicated strategy in order to derive a solution. First, it is discussed how to deal with the intractability of the problem via a sigmoid-based approximation and then an optimization algorithm is proposed.

IV. Sigmoid-Based Approximation

In order to tackle the intractability of the probability $p_{n,k}$ and fidelity $f_{n,k}$, approximations based on the sigmoid function

$$\mathcal{S}(b_1, b_2, b_3, x) \triangleq \frac{b_1}{1 + e^{b_2 + b_3 x}}, \tag{9}$$

are proposed hereby. Indeed, these expressions share three important characteristics: (i) the codomain is bounded between 0 and 1, (ii) both are decreasing for increasing E2E distance, until convergence to zero, and (iii) they exhibit a near-stationary maximum for small values of $d_{t,n,k}$. These mirrored S-shaped functions are good candidates to be approximated via a sigmoid-based data regression approach [50]. For convenience, the proposed model takes into account the E2E distance in place of the UAV position

$$p_{n,k} \simeq \mathcal{S}(\theta_1, \theta_2, \theta_3, d_{n,k}), \tag{10}$$

$$f_{n,k} \simeq \mathcal{S}(\theta'_1, \theta'_2, \theta'_3, d_{n,k}), \tag{11}$$

with $\{\theta_1, \theta_3, \theta'_1, \theta'_3\} > 0$ and $\{\theta_2, \theta'_2\} < 0$.

The resulting approximations are shown in Figure 2 considering two configurations: (i) $C^2 = 10^{-13}$ m$^{-2/3}$ for strong turbulence and $\ell = 1550$ nm, and (ii) $C^2 = 5 \cdot 10^{-14}$ m$^{-2/3}$ for weak turbulence and $\ell = 700$ nm. Specifically, the curves are obtained through trust-region-reflective algorithm [51]. The latter clearly provides remarkable accuracy for both $p_{n,k}$ and

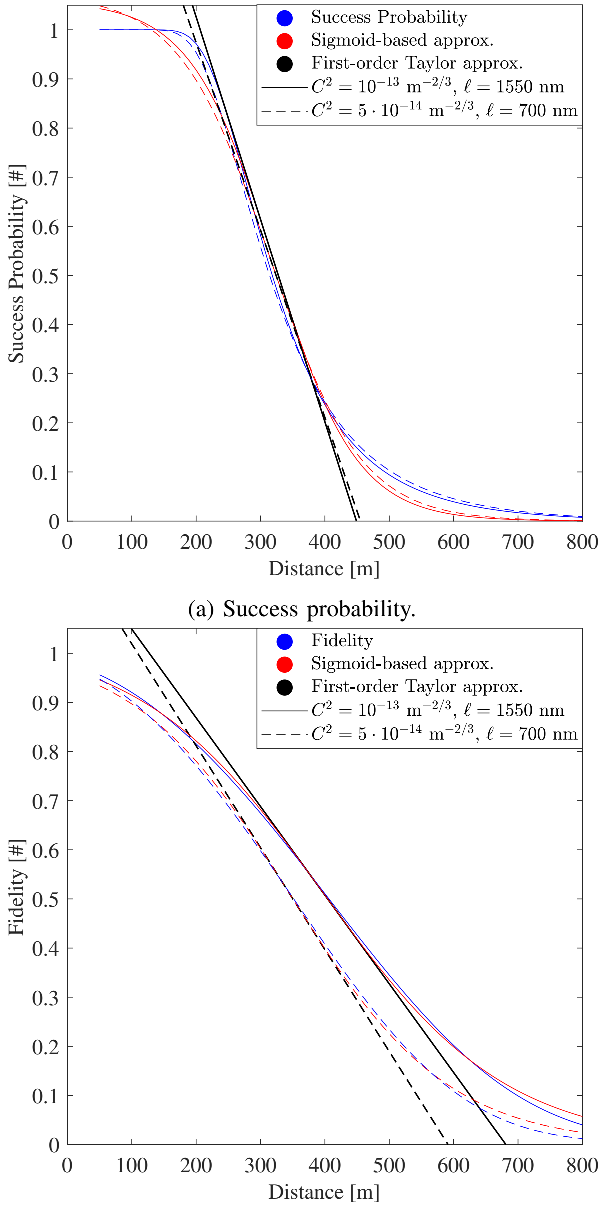

(a) Success probability.

(b) Fidelity.

Fig. 2: Overlook of the probability and fidelity expressions and related approximations.

$f_{n,k}$ with a RMSE in every case lower than 0.03. Differently from the fidelity, the success probability is only slightly affected by the considered parameters. Given the sigmoid-based approximation of the fidelity function in (11), the E2E distance which satisfies the minimum fidelity threshold can be derived as:

$$d_{MAX} \leq \frac{1}{\theta_3'}\left[\ln\left(\frac{\theta_1'}{f_{\min}}-1\right)-\theta_2'\right]. \qquad (12)$$

In practical deployments, this formulation implicitly determines the maximum horizontal extension of the region to cover, given a fixed UAV altitude.

Still, the optimization problem presents challenges due to the change of sign in the second derivative of the sigmoid function in (9), which leads to a shift in convexity at the following inflection point*:

$$\frac{\mathrm{d}^2\mathcal{S}}{\mathrm{d}x^2} = (b_3/b_1)^2\mathcal{S}(\mathcal{S}-b_1)(2\mathcal{S}-b_1) = 0 \implies s = -b_2/b_3.$$

To address the non-convexity of the sigmoid function, SCA technique is employed, which iteratively replaces the non-convex function with a locally valid convex approximation. Specifically, the sigmoid function is linearized using its first-order Taylor expansion at a given local expansion point x_0, obtaining:

$$\mathcal{S} \simeq \mathcal{S}_0 + (b_3/b_1)\mathcal{S}_0(\mathcal{S}_0 - b_1)(x - x_0) \triangleq \widetilde{\mathcal{S}}, \qquad (13)$$

where $\mathcal{S}_0 \triangleq \mathcal{S}(b_1, b_2, b_3, x_0)$ and x_0 stands for the local expansion point. For practical visualization, in Figure 2 the black lines tangent to the sigmoids represent $\widetilde{\mathcal{S}}$ centered around $x_0 = s$. The SCA framework ensures that at each iteration, a convex sub-problem is solved, gradually refining the solution while maintaining feasibility†. Convergence in this context refers to the iterative update of the local expansion point x_0, which leads to progressively improved approximations until the optimization variables stabilize within a predefined tolerance ϵ. Please note that for the sake of numerical stability, it is useful to normalize the argument of the sigmoid to unity, thus allowing a tighter approximation in the local point.

V. Proposed Optimization Algorithm

In this Section, an optimization algorithm is proposed to solve problem (8). Although a tractable sigmoid-based expression has been deduced for fidelity and probability of success, the challenges outlined in Section III remain. To address this, we propose a sequential decomposition into three sub-problems, each of which tackles a specific aspect of the original formulation. This decomposition is motivated by the inherent structure of the problem: fidelity constraints impose strict feasibility requirements, probability of success depends on these feasibility conditions, and data rate optimization is constrained by both. Therefore, the order of the sub-problems is not arbitrary, rather it is driven by feasibility constraints and structural dependencies, as further detailed below.

1) **Fidelity coverage maximization:** This step addresses the most critical requirement in quantum communication — ensuring that each UAV-QN link satisfies a minimum fidelity constraint $f_{n,k} \geq f_{\min}$. The positions of the UAVs are optimized to fairly maximize the number of links which can satisfy the minimum fidelity requirement for each QN. This step determines the set of valid UAV-QN pairs and enables the construction of a binary association matrix, which maps QNs to the UAV that provides the highest fidelity. In this way, QNs are divided

*Technically, a zero second derivative alone does not necessarily indicate an inflection point, as it could also correspond to an undulation point. However, it can be verified that the second derivative exhibits opposite signs in the neighborhood of the solution, confirming that it is indeed the first case.

†Interestingly, instead of iteratively updating the local point with the previous solution, thus moving the tangent line along the sigmoid function, a low-complexity strategy involves only the Taylor expansion centered in the inflection point s, as shown in Figure 2.

into clusters centered on UAVs, laying the foundation for all subsequent optimization.

2) **Success probability maximization:** Once a fidelity-feasible topology is established, UAV positions are further refined to maximize the probability of successfully transmitting entangled photons, i.e., the success probability $p_{n,k}$. Importantly, fidelity constraints remain enforced during this step to ensure continued feasibility. This sub-problem benefits from the reduced complexity introduced by prior clusterization, as only valid UAV-QN links are considered.

3) **Photon rate allocation:** With feasible and high-quality links in place, the final sub-problem focuses on fair resource distribution. The objective is to maximize the minimum number of photons received by each QN, subject to total photon generation capacity (R_{MAX}) and the per-UAV serving limit (K_{MAX}). When the K_{MAX} constraint is relaxed, the problem admits a closed-form solution based on proportional rate allocation, offering structural insight into the optimal allocation policy.

Changing the order of these sub-problems would violate their logical and structural dependencies. For instance, solving rate allocation before verifying fidelity feasibility could result in assigning resources to links that are fundamentally unusable. Similarly, maximizing the success probability before checking fidelity can misdirect UAVs to areas where communication is physically infeasible. Therefore, the adopted sequence ensures that each sub-problem builds upon a validated and feasible solution space established in the previous step.

In the following the probability of successfully receive a photon and the fidelity of the corresponding entangled state are employed combining the sigmoid-based regression in (10) and (11), and the first-order Taylor expansion in (13):

$$\overline{p}_{n,k} \simeq \widetilde{\mathcal{S}}(\theta_1, \theta_2, \theta_3, d_{n,k}, \overline{d}_{n,k}), \tag{14}$$

$$\overline{f}_{n,k} \simeq \mathcal{S}(\theta'_1, \theta'_2, \theta'_3, d_{n,k}, \overline{d}_{n,k}), \tag{15}$$

Please note that both are functions of the distances $\mathbf{D} = \{d_{n,k}\}$ and the local expansion points $\overline{\mathbf{D}} = \{\overline{d}_{n,k}\}$, even if the dependence is omitted for brevity. The complexity and optimality trade-offs of this sequential approach will be further analyzed in Section VI.

A. Sub-problem 1: Fidelity Coverage Maximization

In order to maximize the number of links which provide a minimum fidelity f_{min} for each QN, a set of auxiliary variables $\mathbf{W} = \{w_{n,k}\}$ is employed to model the difference between the fidelity and the target one. Then, the heaviside function can be used to count the number of useful links ($w_{n,k} \geq 0$) as $\sum_{n=1}^{N} \mathcal{H}(w_{n,k})$ for each QN k. According to [52], the Heaviside function $\mathcal{H}(\cdot)$ can be accurately approximated through a sigmoid function since

$$\lim_{\gamma \to +\infty} \mathcal{S}(1, 0, -\gamma, x) = \mathcal{H}(x), \tag{16}$$

where γ is the constant denoting the magnitude of the slope. Leveraging the first-order Taylor approximation in (13) with the SCA technique, the first sub-problem reads

$$\max_{\eta, \mathbf{Q}, \mathbf{D}, \mathbf{W}} \eta \quad s.t. \tag{17}$$

$$\eta \leq \sum_{n=1}^{N} \widetilde{\mathcal{S}}(1, 0, -\gamma, w_{n,k}, \overline{w}_{n,k}), \quad \forall k = 1, \ldots, K, \tag{17a}$$

$$w_{n,k} \leq \overline{f}_{n,k} - f_{min}, \quad \forall n = 1, \ldots, N, \forall k = 1, \ldots, K, \tag{17b}$$

$$\|\hat{\mathbf{q}}_n - \mathbf{u}_k\| + \|\hat{\mathbf{q}}_n - \mathbf{b}\| \leq d_{n,k}, \quad \begin{array}{l} \forall n = 1, \ldots, N, \\ \forall k = 1, \ldots, K, \end{array} \tag{17c}$$

where $\hat{\mathbf{q}}_n = [\mathbf{q}_n, z]^\mathsf{T}$, and $\overline{\mathbf{W}} = \{\overline{w}_{n,k}\}$ is the set containing the values of $\mathbf{W}$ at the previous iteration. The new constraint (17c) is necessary to deal with the regression model adopted, which depends on the E2E distance. Please note that the above sub-problem (17) not only maximizes the number of links which satisfy the minimum target fidelity, but also maximizes the fidelity itself. Indeed, a higher $w_{n,k}$ leads to a higher value on the right hand side of constraint (17a). Moreover, it can be verified that the above formulation is convex and can be iteratively solved until convergence to a prescribed accuracy.

B. Sub-problem 2: Receiving Probability Maximization

Based on the derived solution, the QNs are divided in clusters $\mathbf{U}_n = \{k | f_{n,k} = \max_n(\{f_{n,k}\})\}$ served by the drone which provides the maximum possible fidelity. This UAV-QN association can be expressed through a set of binary variables $a_{n,k} \in \{0, 1\}$. Recalling the definitions of $\overline{p}_{n,k}$ and $\overline{f}_{n,k}$ in (14) and (15), for each UAV (and cluster) n, the second sub-problem reads:

$$\max_{\eta, \mathbf{q}_n, \mathbf{D}_n} \eta \quad s.t. \tag{18}$$

$$\eta \leq \overline{p}_{n,k}, \quad \forall k \in \mathbf{U}_n, \tag{18a}$$

$$\overline{f}_{n,k} \geq f_{min}, \quad \forall k \in \mathbf{U}_n, \tag{18b}$$

where $\mathbf{D}_n$ contains all the K E2E distances given a UAV n, which leads to the obvious definition of $\overline{\mathbf{D}}_n$. It can be verified that the above formulation is convex and can be easily solved through a standard optimization tool as CVX [53]. After the first two sub-problems have been solved, the optimal positions $\mathbf{Q}$ are known and can be leveraged to deduce the optimal photon distribution, discussed in the following sub-section.

C. Sub-problem 3: QBS Data Rate Optimization

First, note that the zero-norm in (8d) can be reformulated as

$$\sum_{k=1}^{K} \mathcal{H}(r_{t,n,k}) \leq K_{MAX}, \ \forall t = 1, \ldots, T, \forall n = 1, \ldots, N. \tag{19}$$

Similarly to the first sub-problem, the heaviside function is substituted with a sigmoid-based approximation. Nonetheless, there are cases in which $r_{t,n,k} = 0$, i.e., $\mathcal{H}(r_{t,n,k}) = 1/2$. Since the data rate is a positive quantity, the constraint require a normalization to unity, i.e., $2\mathcal{H}(r_{t,n,k}) - 1$. Let $\overline{\mathbf{R}} = \{\overline{r}_{t,n,k}\}$

be the set of the local expansion for $\mathbf{R}$. Then, the final formulation of the third sub-problem reads:

$$\max_{\eta,\mathbf{R}} \eta \quad s.t. \tag{20}$$

$$\eta \leq \sum_{t=1}^{T}\sum_{n=1}^{N} a_{n,k} p_{n,k} r_{t,n,k}, \quad \forall k = 1, \ldots, K, \tag{20a}$$

$$\sum_{n=1}^{N}\sum_{k=1}^{K} r_{t,n,k} \leq R_{MAX}, \quad \forall t = 1, \ldots, T, \tag{20b}$$

$$2\sum_{k=1}^{K} \widetilde{\mathcal{S}}(1, 0, -\gamma, r_{t,n,k}, \overline{r}_{t,n,k}) \leq K_{MAX} + K, \quad \begin{array}{l}\forall t = 1, \ldots, T,\\ \forall n = 1, \ldots, N,\end{array} \tag{20c}$$

which can be now solved with standard optimization software as CVX. Note that, thanks to the UAV position optimization performed in the previous steps, constraint (8b) does not appear in the formulation because the UAV-QN useful links have been already deduced.

It is worth specifying that in case of $K_{MAX} = K$, constraint (20c) can be neglected, as there is no upper bound on the number of QNs a IRS-equipped UAV can serve. As a result, the problem simplifies significantly, allowing to derive a time-invariant closed-form solution using the Karush-Kuhn-Tucker (KKT) conditions, similar to [13, Theorem 1]:

$$r_{n,k} = R_{MAX} \left(p_{n,k} \sum_{n=1}^{N}\sum_{k=1}^{K} \frac{a_{n,k}}{p_{n,k}} \right)^{-1}. \tag{21}$$

Notably, in the absence of an upper limit on served QNs, the solution becomes purely proportional to the weighted probabilities $p_{n,k}$. This means that the allocation is dictated solely by the relative probability distribution, rather than by any time-dependent constraints. Consequently, there is no need for dynamic resource allocation across time slots, since UAVs are no longer constrained and can distribute the resources to all QNs in their cluster. This implies that the solution becomes static, meaning the same allocation can be applied at each timeslot t without the need for further optimization.

VI. Algorithm Complexity, Optimality, and Convergence

The overall algorithm is summarized in Algorithm 1. The complexity of the first sub-problem is $\mathcal{O}\big(I_1(2N(1+K)+1)^{3.5}\big)$, the second one is $\mathcal{O}\big(I_2 N(K+3)^{3.5}\big)$, while the third one is $\mathcal{O}\big(I_3(TNK+1)^{3.5}\big)$, with I_1, I_2, and I_3 being the maximum number of iterations required by the SCA. Therefore, the total time complexity corresponds to $\simeq \mathcal{O}\big((I_1+I_2+I_3)(NK(2+T))^{3.5}\big)$.

The proposed strategy does not guarantee global optimality due to two main factors: (i) the linear approximation of the sigmoidal functions, which introduces an inherent approximation error, and (ii) the sequential decomposition of the original problem, which may lead to suboptimal intermediate solutions. Moreover, it is worth specifying that multiple global optimal solutions can exist given certain simulation parameters. Despite these limitations, we will numerically demonstrate that the algorithm consistently converges and provides high-quality solutions, highlighting its practical effectiveness in relevant scenarios.

Algorithm 1: Proposed Optimization Algorithm

```
Input: Number of nodes K and their positions u_k,
   QBS location b, minimum fidelity f_min;
Output: Optimal UAVs positions Q, optimal photon
   distribution R;
Compute the sigmoid-based fitting according to (10)
   and (11) and the corresponding expansions in (13);
Randomly initialize local points D̄ and W̄;
do
    Solve (17) to obtain η, Q, D, and W;
    D̄ ← D; W̄ ← W;
while until convergence;
Divide the QNs in clusters served by a single UAV n
   based on the highest possible fidelity;
for n = 1 to N do
    do
        Solve (18) to obtain η, q_n, and D_n;
        D̄_n ← D_n;
    while until convergence;
end
Compute the probability of success p̄_{n,k} and fidelity
   f̄_{n,k} according to the derived positions Q;
do
    Solve (20) to obtain η, and R;
    R̄ ← R;
while until convergence;
```

For what concerns convergence, the overall algorithm proceeds through a fixed sequence of three sub-problems (fidelity coverage, success probability maximization, and data rate allocation), each one handled via SCA. Formally, at every iteration, each non-convex sigmoid term is replaced by a convex surrogate obtained by first-order Taylor expansion around the current expansion point. This surrogate satisfies the standard conditions required for SCA convergence: (i) it is a global upper bound of the original function in the feasible region, (ii) it is tight at the current expansion point (function value and gradient match), and (iii) it is convex and continuously differentiable. Under these assumptions, SCA iterations are guaranteed to converge to a stationary point of the corresponding non-convex sub-problem [54].

We emphasize that this guarantee holds for each sub-problem separately. Since the three sub-problems are solved sequentially in a block-coordinate fashion, the overall three-stage procedure should be regarded as a heuristic decomposition method rather than a globally convergent optimization scheme. Nevertheless, in our numerical experiments the method consistently converges in a few iterations and provides significantly better performance than baseline approaches.

VII. Numerical Results and Discussion

In this Section a simulation campaign is carried out to assess the effectiveness of the proposed solution. Specifically, the tests are conducted on a Intel Core i7-13800H with 32 GB

Parameter	Value	Parameter	Value
K	16 [#]	f_{min}	0.8
b	$[0, 200, 0]^\mathsf{T}$ $[m]$	z	50 $[m]$
ℓ	1550 $[nm]$	K_{MAX}	$\{1, K\}$
T	20 [#]	ζ_{th}	0.05
δ	1 $[s]$	ς	0.97
C^2	1×10^{-13} $[m^{-2/3}]$	ν	0.95
R_{MAX}	1 $[kHz]$	$\lambda_{00,i}$	0.99
τ	4 $[\mu s]$	τ_{coh}	2.43 $[ms]$
N	$\{1, \ldots, 6\}$ [#]	ϵ	1×10^{-4}

TABLE II: Main parameters of the simulation campaign.

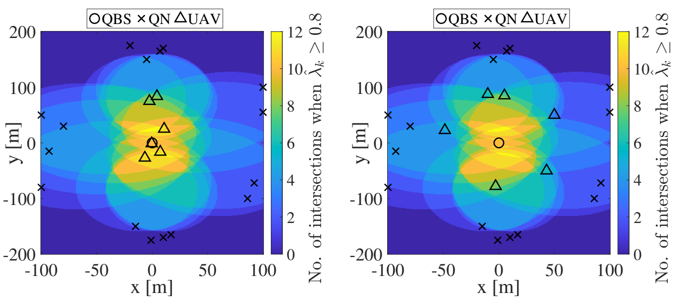

(a) First sub-problem. (b) Second sub-problem.

Fig. 3: First scenario: UAV hovering positions.

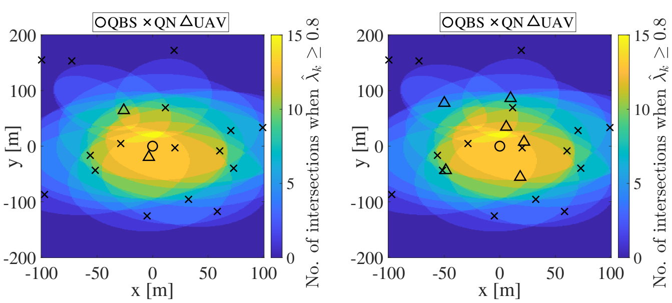

(a) $N = 2$ (b) $N = 6$

Fig. 4: Second scenario: final UAV hovering positions.

of RAM. The investigated scenarios consider a QBS located at $\mathbf{b} = [0, 0, 0]^\mathsf{T}$ m within a 3D grid, serving $K = 16$ quantum nodes deployed on the ground over an area of 200x400 m^2. The selection of this area size is driven by the requirement to ensure that the distributed entangled photons maintain a minimum fidelity f_{min} of 0.8. To assist the distribution of the entangled pairs, the locations of the IRS-equipped UAVs are optimized at fixed altitude $z = 50$ m.

For the optical channel, the considered configuration parameters can be found in [40], except that in this work it is considered a moderate-strong turbulence, i.e., $C^2 = 1{\times}10^{-13}\text{m}^{-2/3}$. Therefore, the success probability and fidelity curves are approximated as discussed in Section IV with the following parameters $\{\theta_1, \theta_2, \theta_3\} = \{1.06, -5, 0.015\}$ and $\{\theta_1', \theta_2', \theta_3'\} = \{1.03, -2.78, 0.007\}$. The QBS can generate entanglement at a maximum rate of $R_{MAX} = 1$ kHz with an initial fidelity of $\lambda_{00,i} = 0.99$, as demonstrated by the rate-fidelity trade-off [55]. Unless otherwise specified, all parameters are summarized in Table II.

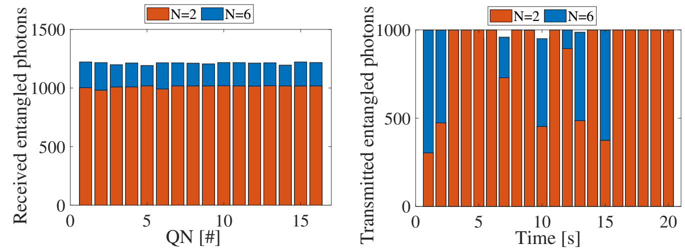

(a) Received photons. (b) Transmitted photons.

Fig. 5: Second scenario: received and transmitted photons.

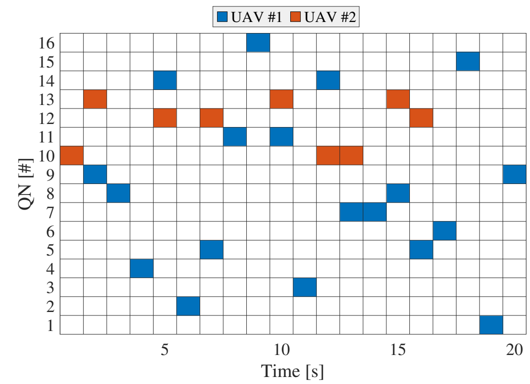

(a) $N = 2$.

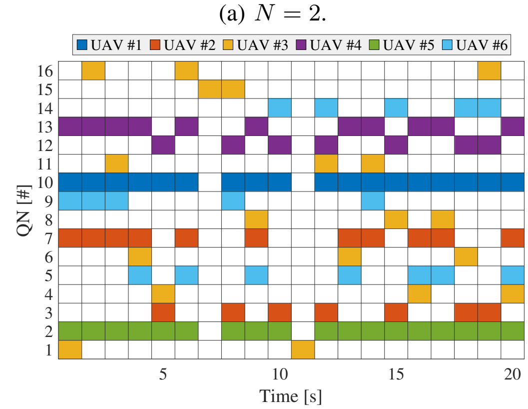

(b) $N = 6$.

Fig. 6: Scheduling for the second scenario with $K_{MAX} = 1$.

A. Optimal UAVs' positions analysis

In the first analyzed scenario, a swarm of $N = 6$ IRS-equipped UAV assists the communication between the QBS and the QNs. The overall scenario is depicted in Fig. 3, which shows the positions obtained from the first two sub-problems and the locations of the QNs and the QBS. The heatmap in the background is generated by computing the fidelity between the QBS and each QN for every point in the 2D grid (UAV position), highlighting the number of intersections where the fidelity exceeds $f_{min} = 0.8$. As it can be seen, in the first step, the UAVs are positioned closer to the base station, where they are able to satisfy the minimum fidelity requirement for a greater number of QNs. Instead, in the second stage after the clusters have been identified, the positions are closer to the QNs that have to be served to maximize the probability of

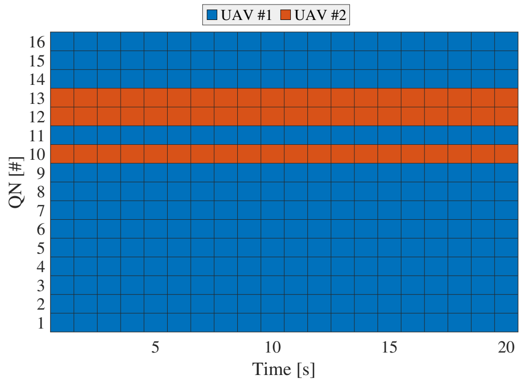

(a) $N = 2$.

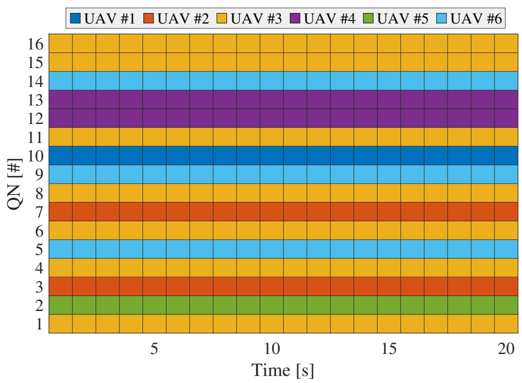

(b) $N = 6$.

Fig. 7: Scheduling for the second scenario with $K_{MAX} = K$.

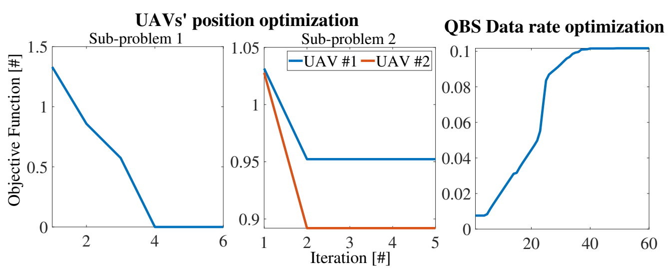

Fig. 8: Convergence of the algorithms with $N = 2$.

success by lowering the E2E distance.

To further validate the proposed approach, in the second scenario, a new random QN configuration is employed. Moreover, to analyze the impact of the number of UAVs employed, $N = \{2, 6\}$ is selected. Fig. 4 shows the final UAV hovering positions, i.e., second sub-problem. Clearly, in case of a lower number of UAVs, the latter must hover over regions that guarantee a sufficiently high number of QNs served simultaneously that satisfy the fidelity constraint and, at the same time, maximizes the probability of successfully receive photons. On the contrary, in the case of $N = 6$, the UAVs are more uniformly spread over the entire area, thus maximizing the data rate.

B. Sum-rate and convergence analysis

Given the configuration depicted in Fig. 4, Figs. 5a and 5b show the total amount of received entangled photons at the end of the mission for each QN and the total amount of entangled photons transmitted by the QBS, respectively. It can be observed that by the end of the mission, all the QNs received approximately the same number of entangled photons, demonstrating satisfactory results in terms of fairness in both configurations. However, in case of $N = 6$, the sum-rate achieved, i.e., ~ 1212 pairs per second, is 19% higher with respect to the setup with $N = 2$, i.e., ~ 1018. Moreover, for $N = 6$, the QBS consistently generates and transmits at near-maximum capacity throughout the mission. Instead, in the other configuration, this is not the case since transmitting more photons would have resulted in an unfair distribution.

To provide further insights on this aspect, Fig. 6 illustrates the scheduling plan of the two configurations for $K_{MAX} = 1$. As can be seen, in case of $N = 2$ the clusterization process assigned 13 QNs to UAV #1 and 3 QNs to UAV #2. Therefore, the majority of the time intervals are entirely dedicated to single users of the first cluster, which need a higher number of photons overall. As a such, to guarantee the fairness, the transmissions related to the second cluster are not only limited in terms of transmitted photons (as can be seen in Fig. 5b) but are also performed in parallel with the ones of the first cluster. On the contrary, a more even distribution of the QNs is possible in the $N = 6$ configuration, as can be seen through the scheduling depicted in Fig. 6b. This results in a more even resource distribution, and in turn in a higher sum-rate. Indeed, when there are many little clusters, each UAV position can be optimized to better maximize the success probability by lowering the E2E distances.

For the sake of completeness, the scheduling plans for the case in which $K_{MAX} = K$, i.e, unbounded case, are reported in Fig. 7. These are depicted by ignoring constraint (8d), which leads to a simpler form of the third sub-problem. The latter admits the closed-form solution in (21) that does not depend on the time. Indeed, there is no limitation on the number of simultaneous links that a UAV can serve. In this case, both the configuration reach the same data rate for all the QNs of 1243 pairs per second.

Finally, Fig. 8 shows the convergence curves of the proposed optimization algorithm in all sub-problems, in terms of objective function values. It can be noted that in the first two sub-problems converge in very few iterations, while the third one more iterations are required. Nonetheless, the whole optimization process lasts less than two minutes in every tested parameter setting.

C. Baseline comparison

In this final analysis, two separate investigations are carried out to evaluate the performance of the proposed approach under different conditions.

First, the impact of varying the number of UAVs is analyzed with fixed $K_{MAX} = 1$, and results are compared against two baseline approaches. Both baselines derive the UAV positions using a weighted k-means clustering algorithm [56]. Initially, UAV positions are randomly initialized. Then, the QNs are assigned to the cluster of the closest UAV, where the distances are weighted according to the inverse of the

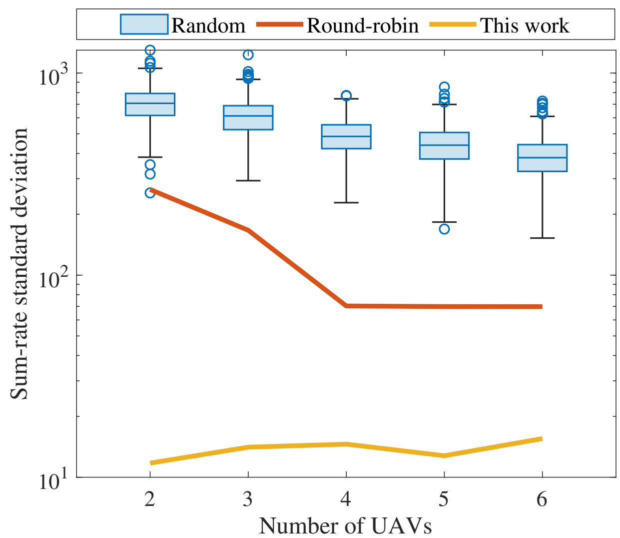

Fig. 9: Comparison between proposed and baseline approaches with respect to the fairness.

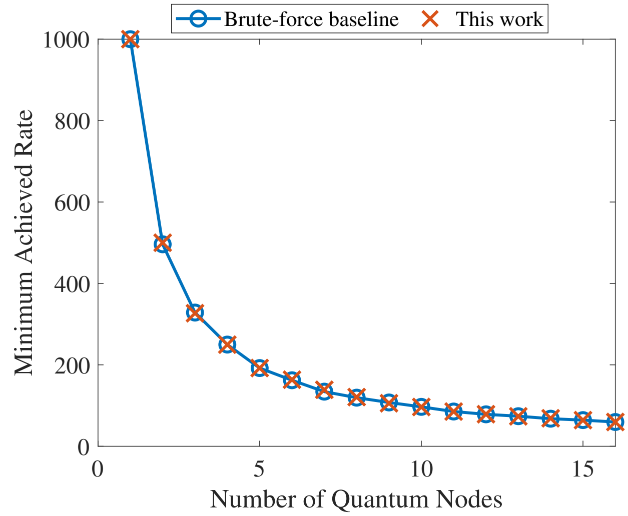

Fig. 10: Comparison between proposed solution and brute-force grid-based baseline.

QN-QBS distances. This ensures that the farthest nodes from the QBS are prioritized in the assignment. Finally, the UAV positions are updated as the centroid of their cluster, where the latter also accounts for the QBS position. Here, the UAV position of the E2E links that fail to meet the minimum fidelity requirement are iteratively adjusted. This process moves those locations towards the direction of the QN if the UAV-QN distance is greater than the UAV-QBS one, and closer to the QBS otherwise.

Once the positions are derived, a different approach for the resource distribution is followed by the two baselines:

- Random: All the pairs R_{MAX} are randomly assigned to QNs according to a uniform distribution. A Monte Carlo experiment with 1000 samples is carried out in this case.
- Round-robin: The EPR pairs are distributed to each cluster according to $R_{MAX}K_n/K$, where K_n is the number of QNs of each cluster. The partitioned EPR couples are then transmitted to each QN of the clusters in a round-robin fashion.

The standard deviation computed on the sum-rate of the nodes is adopted as metric of reference to measure the fairness. As can be seen in Fig. 9, the proposed solution enhances overall performance by at least an order of magnitude, thus ensuring a more equitable distribution of resources among the nodes. The proposed approach exhibits immediately an almost-constant trend, whereas both the baselines show a decreasing trend. This demonstrates that the proposed approach is able to guarantee a quasi-optimal distribution independently of the number of the UAVs. On the contrary, both baselines benefit from the presence of more UAVs, which however is not sufficient to reach the performance of the proposal. In case of the round-robin approach, the curve saturates when the number of UAVs reaches four, over which no improvements are observed.

In this second analysis, we consider a complementary baseline based on a brute-force grid search, applied under the assumption $K = K_{MAX}$. Here, the number of UAVs is fixed to $N = 3$, while the number of QNs varies according to a uniform random topology. Then, the UAV positions are exhaustively selected from a discrete grid with spatial resolution $\delta = 10$ m. For each configuration, QNs are assigned to the UAV with the highest success probability, subject to the fidelity constraint. The rate allocation is computed using the closed-form max-min fairness expression valid under $K = K_{MAX}$ in (21). The resulting minimum rate across all QNs is reported. This brute-force grid-based strategy serves as an upper-bound reference, allowing direct comparison to the proposed optimization method. As shown in Fig. 10, the latter matches the performance of the brute-force grid-based baseline across all values of k in terms of the minimum achieved rate. This result demonstrates that the proposed method, despite its significantly lower computational complexity, effectively captures the structure of the problem and delivers near-optimal performance even when compared to an exhaustive search.

VIII. Conclusions

In this work, a FSO-based quantum network assisted by multiple IRS-equipped UAVs has been first modeled in terms of success probability and fidelity of received states and then optimized to achieve a fair distribution of the available resources. The formulated optimization problem, originally presented tractability issues due to the presence of the Heaviside step function and the ℓ_0-norm in some constraints. A sigmoid-based approximation strategy combined with the BCD and SCA techniques has been developed to cope with the non-convexity of the initial formulation, which led to an optimization algorithm, whose complexity and optimality have been analyzed. The conducted simulation campaign clearly indicates that the links-per-IRS and number of drones must be fine-tuned on the specifics of the scenario to achieve optimal performance. The proposed solution demonstrated an order of magnitude increase in fairness compared to the first two baselines, while consistently achieving optimal minimum rates when compared with the third one. Future works include the analysis of more complex multi-hop networks, where a swarm of UAVs with swapping and IRS mixed capabilities can assist connectivity of QNs on the ground.

REFERENCES

[1] P. Zhang, N. Chen, S. Shen, S. Yu, S. Wu, and N. Kumar, "Future quantum communications and networking: A review and vision," *IEEE Wireless Communications*, vol. 31, no. 1, pp. 141–148, 2024.

[2] Z. Yang, M. Zolanvari, and R. Jain, "A survey of important issues in quantum computing and communications," *IEEE Communications Surveys & Tutorials*, vol. 25, no. 2, pp. 1059–1094, 2023.

[3] J. Illiano, M. Caleffi, A. Manzalini, and A. S. Cacciapuoti, "Quantum internet protocol stack: A comprehensive survey," *Computer Networks*, vol. 213, p. 109092, 2022.

[4] L. Gyongyosi and S. Imre, "A survey on quantum computing technology," *Computer Science Review*, vol. 31, pp. 51–71, 2019.

[5] A. S. Cacciapuoti, M. Caleffi, F. Tafuri, F. S. Cataliotti, S. Gherardini, and G. Bianchi, "Quantum internet: Networking challenges in distributed quantum computing," *IEEE Network*, vol. 34, no. 1, pp. 137–143, 2019.

[6] M. Caleffi, M. Amoretti, D. Ferrari, D. Cuomo, J. Illiano, A. Manzalini, and A. S. Cacciapuoti, "Distributed quantum computing: a survey," *arXiv preprint arXiv:2212.10609*, 2022.

[7] F. Vista, S. DiAdamo, E. Kaur, H. Shapourian, and R. Nejabati, "Entanglement request scheduling in quantum datacenter networks," *IEEE Network*, pp. 1–1, 2025.

[8] V. Scarani, H. Bechmann-Pasquinucci, N. J. Cerf, M. Dušek, N. Lütkenhaus, and M. Peev, "The security of practical quantum key distribution," *Reviews of modern physics*, vol. 81, no. 3, p. 1301, 2009.

[9] P. W. Shor and J. Preskill, "Simple proof of security of the bb84 quantum key distribution protocol," *Physical review letters*, vol. 85, no. 2, p. 441, 2000.

[10] M. Mehic, M. Niemiec, S. Rass, J. Ma, M. Peev, A. Aguado, V. Martin, S. Schauer, A. Poppe, C. Pacher *et al.*, "Quantum key distribution: a networking perspective," *ACM Computing Surveys (CSUR)*, vol. 53, no. 5, pp. 1–41, 2020.

[11] X.-M. Hu, Y. Guo, B.-H. Liu, C.-F. Li, and G.-C. Guo, "Progress in quantum teleportation," *Nature Reviews Physics*, vol. 5, no. 6, pp. 339–353, 2023.

[12] D. Bouwmeester, J.-W. Pan, K. Mattle, M. Eibl, H. Weinfurter, and A. Zeilinger, "Experimental quantum teleportation," *Nature*, vol. 390, no. 6660, pp. 575–579, 1997.

[13] G. Iacovelli, F. Vista, N. Cordeschi, and L. A. Grieco, "A probability-based optimization approach for entanglement distribution and source position in quantum networks," *IEEE Journal on Selected Areas in Communications*, vol. 42, no. 7, pp. 1738–1748, 2024.

[14] R. Quan, H. Hong, W. Xue, H. Quan, W. Zhao, X. Xiang, Y. Liu, M. Cao, T. Liu, S. Zhang, and R. Dong, "Implementation of field two-way quantum synchronization of distant clocks across a 7 km deployed fiber link," *Opt. Express*, vol. 30, no. 7, pp. 10 269–10 279, Mar 2022.

[15] R. Jozsa, D. S. Abrams, J. P. Dowling, and C. P. Williams, "Quantum clock synchronization based on shared prior entanglement," *Physical Review Letters*, vol. 85, no. 9, p. 2010, 2000.

[16] X. Guo, C. R. Breum, J. Borregaard, S. Izumi, M. V. Larsen, T. Gehring, M. Christandl, J. S. Neergaard-Nielsen, and U. L. Andersen, "Distributed quantum sensing in a continuous-variable entangled network," *Nature Physics*, vol. 16, no. 3, pp. 281–284, 2020.

[17] R. Horodecki, P. Horodecki, M. Horodecki, and K. Horodecki, "Quantum entanglement," *Reviews of modern physics*, vol. 81, no. 2, p. 865, 2009.

[18] Z. Li, K. Xue, J. Li, L. Chen, R. Li, Z. Wang, N. Yu, D. S. L. Wei, Q. Sun, and J. Lu, "Entanglement-assisted quantum networks: Mechanics, enabling technologies, challenges, and research directions," *IEEE Communications Surveys & Tutorials*, vol. 25, no. 4, pp. 2133–2189, 2023.

[19] B.-C. Ciobanu, L. P. Verzotti, and P. G. Popescu, "Optimal and scalable entanglement distribution over crossbar quantum networks," *Scientific Reports*, vol. 14, no. 1, p. 11714, 2024.

[20] M. G. Kuzyk, "Quantum no-cloning theorem and entanglement," *American Journal of Physics*, vol. 87, no. 5, pp. 325–327, 05 2019.

[21] A. Singh, K. Dev, H. Siljak, H. D. Joshi, and M. Magarini, "Quantum internet—applications, functionalities, enabling technologies, challenges, and research directions," *IEEE Communications Surveys & Tutorials*, vol. 23, no. 4, pp. 2218–2247, 2021.

[22] K. Azuma, S. E. Economou, D. Elkouss, P. Hilaire, L. Jiang, H.-K. Lo, and I. Tzitrin, "Quantum repeaters: From quantum networks to the quantum internet," *Reviews of Modern Physics*, vol. 95, no. 4, p. 045006, 2023.

[23] J.-W. Pan, D. Bouwmeester, H. Weinfurter, and A. Zeilinger, "Experimental entanglement swapping: entangling photons that never interacted," *Physical review letters*, vol. 80, no. 18, p. 3891, 1998.

[24] Á. G. Iñesta, G. Vardoyan, L. Scavuzzo, and S. Wehner, "Optimal entanglement distribution policies in homogeneous repeater chains with cutoffs," *npj Quantum Information*, vol. 9, no. 1, p. 46, 2023.

[25] L. de Forges de Parny, O. Alibart, J. Debaud, S. Gressani, A. Lagarrigue, A. Martin, A. Metrat, M. Schiavon, T. Troisi, E. Diamanti *et al.*, "Satellite-based quantum information networks: use cases, architecture, and roadmap," *Communications Physics*, vol. 6, no. 1, p. 12, 2023.

[26] S. Pirandola, "Limits and security of free-space quantum communications," *Physical Review Research*, vol. 3, no. 1, p. 013279, 2021.

[27] G. Vallone, D. Bacco, D. Dequal, S. Gaiarin, V. Luceri, G. Bianco, and P. Villoresi, "Experimental satellite quantum communications," *Physical Review Letters*, vol. 115, no. 4, p. 040502, 2015.

[28] J. Yin, Y. Cao, Y.-H. Li, S.-K. Liao, L. Zhang, J.-G. Ren, W.-Q. Cai, W.-Y. Liu, B. Li, H. Dai *et al.*, "Satellite-based entanglement distribution over 1200 kilometers," *Science*, vol. 356, no. 6343, pp. 1140–1144, 2017.

[29] C.-Y. Lu, Y. Cao, C.-Z. Peng, and J.-W. Pan, "Micius quantum experiments in space," *Reviews of Modern Physics*, vol. 94, no. 3, p. 035001, 2022.

[30] H.-Y. Liu, X.-H. Tian, C. Gu, P. Fan, X. Ni, R. Yang, J.-N. Zhang, M. Hu, J. Guo, X. Cao *et al.*, "Drone-based entanglement distribution towards mobile quantum networks," *National science review*, vol. 7, no. 5, pp. 921–928, 2020.

[31] F. Vista, D. Holme, and S. DiAdamo, "Quantum backbone networks for hybrid quantum dataframe transmission," *IEEE Communications Magazine*, vol. 62, no. 10, pp. 28–33, 2024.

[32] X. Wei, J. Liu, L. Fan, Y. Guo, Z. Han, and Y. Wang, "Optimal entanglement distribution problem in satellite-based quantum networks," *IEEE Network*, pp. 1–1, 2024.

[33] A. Kržič, S. Sharma, C. Spiess, U. Chandrashekara, S. Töpfer, G. Sauer, L. J. González-Martín del Campo, T. Kopf, S. Petscharnig, T. Grafenauer *et al.*, "Towards metropolitan free-space quantum networks," *npj Quantum Information*, vol. 9, no. 1, p. 95, 2023.

[34] W. Fang, W. Chen, Q. Wu, K. Wang, S. Zhang, Q. Liu, and J. Li, "Reconfigurable intelligent surface assisted free space optical information and power transfer," *IEEE Internet of Things Journal*, pp. 1–1, 2024.

[35] N. Vishwakarma, R. Swaminathan, P. D. Diamantoulakis, and G. K. Karagiannidis, "Performance analysis of optical reflecting surface-assisted optical space shift keying-based mimo-fso system," *IEEE Transactions on Communications*, vol. 71, no. 8, pp. 4751–4763, 2023.

[36] H.-Y. Liu, X.-H. Tian, C. Gu, P. Fan, X. Ni, R. Yang, J.-N. Zhang, M. Hu, J. Guo, X. Cao *et al.*, "Optical-relayed entanglement distribution using drones as mobile nodes," *Physical Review Letters*, vol. 126, no. 2, p. 020503, 2021.

[37] V. K. Chapala and S. M. Zafaruddin, "Unified performance analysis of reconfigurable intelligent surface empowered free-space optical communications," *IEEE Transactions on Communications*, vol. 70, no. 4, pp. 2575–2592, 2021.

[38] N. K. Kundu, M. R. McKay, R. Murch, and R. K. Mallik, "Intelligent reflecting surface-assisted free space optical quantum communications," *IEEE Transactions on Wireless Communications*, vol. 23, no. 5, pp. 5079–5093, 2024.

[39] S. Kisseleff and S. Chatzinotas, "Trusted reconfigurable intelligent surface for multi-user quantum key distribution," *IEEE Communications Letters*, vol. 27, no. 8, pp. 2237–2241, 2023.

[40] M. Chehimi, M. Elhattab, W. Saad, G. Vardoyan, N. K. Panigrahy, C. Assi, and D. Towsley, "Reconfigurable intelligent surface (ris)-assisted entanglement distribution in fso quantum networks," *IEEE Transactions on Wireless Communications*, pp. 1–1, 2025.

[41] P.-Y. Kong, "Uav-assisted quantum key distribution for secure communications with resource limited devices," *IEEE Transactions on Vehicular Technology*, pp. 1–11, 2024.

[42] N. Alshaer, A. Moawad, and T. Ismail, "Reliability and security analysis of an entanglement-based qkd protocol in a dynamic ground-to-uav fso communications system," *IEEE Access*, vol. 9, pp. 168 052–168 067, 2021.

[43] F. Chiti, R. Picchi, and L. Pierucci, "Metropolitan quantum-drone networking and computing: A software-defined perspective," *IEEE Access*, vol. 10, pp. 126 062–126 073, 2022.

[44] G. Iacovelli, A. Coluccia, and L. A. Grieco, “Multi-uav irs-assisted communications: Multinode channel modeling and fair sum-rate optimization via deep reinforcement learning,” *IEEE Internet of Things Journal*, vol. 11, no. 3, pp. 4470–4482, 2024.

[45] M. Chehimi and W. Saad, “Entanglement rate optimization in heterogeneous quantum communication networks,” in *2021 17th International Symposium on Wireless Communication Systems (ISWCS)*, 2021, pp. 1–6.

[46] M. Ghalaii and S. Pirandola, “Quantum communications in a moderate-to-strong turbulent space,” *Communications Physics*, vol. 5, no. 1, p. 38, 2022.

[47] V. Jamali, D. S. Michalopoulos, M. Uysal, and R. Schober, “Link allocation for multiuser systems with hybrid rf/fso backhaul: Delay-limited and delay-tolerant designs,” *IEEE transactions on wireless communications*, vol. 15, no. 5, pp. 3281–3295, 2016.

[48] C. Cantore, D. Monopoli, A. Altamura, A. Mengali, and M. Grande, “An accurate and efficient numerical tool for the analysis and design of optical feeder links,” in *2023 IEEE 10th International Workshop on Metrology for AeroSpace (MetroAeroSpace)*, 2023, pp. 534–539.

[49] M. A. Nielsen and I. L. Chuang, *Quantum computation and quantum information*. Cambridge university press, 2010.

[50] C. You and R. Zhang, “3d trajectory optimization in rician fading for uav-enabled data harvesting,” *IEEE Transactions on Wireless Communications*, vol. 18, no. 6, pp. 3192–3207, 2019.

[51] A. R. Conn, N. I. Gould, and P. L. Toint, *Trust region methods*. SIAM, 2000.

[52] G. Iacovelli and C. Iacovelli, “Representing logic gates over euclidean space via heaviside step function,” *Scientific Reports*, vol. 12, no. 1, p. 8009, 2022.

[53] M. Grant and S. Boyd, “CVX: MATLAB Software for Disciplined Convex Programming,” 2016. [Online]. Available: http://cvxr.com/cvx

[54] G. Scutari, F. Facchinei, L. Lampariello, and P. Song, “Parallel and distributed methods for nonconvex optimization,” in *2014 IEEE International Conference on Acoustics, Speech and Signal Processing (ICASSP)*, 2014, pp. 840–844.

[55] P. C. Humphreys, N. Kalb, J. P. Morits, R. N. Schouten, R. F. Vermeulen, D. J. Twitchen, M. Markham, and R. Hanson, “Deterministic delivery of remote entanglement on a quantum network,” *Nature*, vol. 558, no. 7709, pp. 268–273, 2018.

[56] H. Liu, J. Wu, T. Liu, D. Tao, and Y. Fu, “Spectral ensemble clustering via weighted k-means: Theoretical and practical evidence,” *IEEE Transactions on Knowledge and Data Engineering*, vol. 29, no. 5, pp. 1129–1143, 2017.